Am J Nucl Med Mol Imaging 2016;6(1):18-31
www.ajnmmi.us /ISSN:2160-8407/ajnmmi0017336

Original Article

Feasibility of ^{68}Ga-labeled Siglec-9 peptide for the imaging of acute lung inflammation: a pilot study in a porcine model of acute respiratory distress syndrome

Jaime Retamal[1,2], Jens Sörensen[3], Mark Lubberink[3], Fernando Suarez-Sipmann[1,4], João Batista Borges[1,5], Ricardo Feinstein[6], Sirpa Jalkanen[7], Gunnar Antoni[8], Göran Hedenstierna[1], Anne Roivainen[9,10], Anders Larsson[1], Irina Velikyan[3]

[1]Department of Surgical Sciences, Hedenstierna laboratory, Uppsala University, Uppsala, Sweden; [2]Departament de Medicina Intensiva, Pontificia Universidad Católica de Chile, Santiago, Chile; [3]Department of Surgical Sciences, Section of Nuclear Medicine and PET, Uppsala University, Uppsala, Sweden; [4]CIBER de Enfermedades Respiratorias, Instituto de Salud Carlos III, Madrid, Spain; [5]Pulmonary Divison, Heart Institute (Incor) Hospital das Clínicas da Faculdade de Medicina da Universidade de São Paulo, Brazil; [6]The Swedish National Veterinary Institute, Sweden; [7]MediCity Research Laboratory, Department of Medical Microbiology and Immunology, University of Turku, Turku, Finland; [8]Department of Medicinal Chemistry, Uppsala University, Uppsala, Sweden; [9]Turku PET Centre, University of Turku and Turku University Hospital, Turku, Finland; [10]Turku Center for Disease Modelling, University of Turku, Furku, Finland

Received October 5, 2015; Accepted December 4, 2015; Epub January 28, 2016; Published January 30, 2016

Abstract: There is an unmet need for noninvasive, specific and quantitative imaging of inherent inflammatory activity. Vascular adhesion protein-1 (VAP-1) translocates to the luminal surface of endothelial cells upon inflammatory challenge. We hypothesized that in a porcine model of acute respiratory distress syndrome (ARDS), positron emission tomography (PET) with sialic acid-binding immunoglobulin-like lectin 9 (Siglec-9) based imaging agent targeting VAP-1 would allow quantification of regional pulmonary inflammation. ARDS was induced by lung lavages and injurious mechanical ventilation. Hemodynamics, respiratory system compliance (Crs) and blood gases were monitored. Dynamic examination using [^{15}O]water PET-CT (10 min) was followed by dynamic (90 min) and whole-body examination using VAP-1 targeting ^{68}Ga-labeled 1,4,7,10-tetraaza cyclododecane-1,4,7-tris-acetic acid-10-ethylene glycol-conjugated Siglec-9 motif peptide ([^{68}Ga]Ga-DOTA-Siglec-9). The animals received an anti-VAP-1 antibody for post-mortem immunohistochemistry assay of VAP-1 receptors. Tissue samples were collected post-mortem for the radioactivity uptake, histology and immunohistochemistry assessment. Marked reduction of oxygenation and Crs, and higher degree of inflammation were observed in ARDS animals. [^{68}Ga]Ga-DOTA-Siglec-9 PET showed significant uptake in lungs, kidneys and urinary bladder. Normalization of the net uptake rate (K_i) for the tissue perfusion resulted in 4-fold higher uptake rate of [^{68}Ga]Ga-DOTA-Siglec-9 in the ARDS lungs. Immunohistochemistry showed positive VAP-1 signal in the injured lungs. Detection of pulmonary inflammation associated with a porcine model of ARDS was possible with [^{68}Ga]Ga-DOTA-Siglec-9 PET when using kinetic modeling and normalization for tissue perfusion.

Keywords: ^{68}Ga, PET, lung inflammation, Siglec-9, VAP-1

Introduction

Acute respiratory distress syndrome (ARDS) is a devastating syndrome with high mortality and morbidity. Main characteristics of ARDS are alveolar collapse and lung inflammation [1]. Lung inflammation in ARDS is a complex process initiated, amplified, and modulated by a wide network of cytokines and other inflammatory mediators secreted by a variety of cell types including inflammatory cells, fibroblasts, endothelial and epithelial cells [2]. However, possibilities to analyze lung inflammation during ARDS are limited because the available techniques are invasive and non-specific [3].

During the last years positron emission tomography-computed tomography (PET-CT) imaging has become an attractive option to study lung inflammation in ARDS because it is noninvasive and has potential for quantification of pulmonary inflammation throughout the lungs [4]. The

most common PET tracer in lung inflammation studies is 2-deoxy-2-[^{18}F]-fluoroglucose ([^{18}F]FDG). It is an analogue of glucose and its uptake reflects the expression of the glucose transporters and activity of hexokinase enzyme, and thus cellular glucose consumption. Neutrophils become highly activated in response to inflammatory stimuli, as it occurs in ARDS, consuming 20-30 times more glucose when activated than at rest [5]. Since the [^{18}F]FDG uptake is determined essentially by the metabolic activity the inflammation can only be referred indirectly from the [^{18}F]FDG uptake [4].

Vascular adhesion protein-1 (VAP-1) is a homodimeric sialoglycoprotein with adhesive and enzymatic functions. Normally it is stored in intracellular granules but upon inflammatory challenge it is rapidly translocated to the luminal surface of endothelial cells. The enzymatic VAP-1 activity modulates potent inflammatory mediators and can up-regulate other adhesion molecules [6, 7]. VAP-1 has been investigated as a potential target for *in vivo* imaging of inflammation by PET [7-12]. Recently, sialic acid-binding immunoglobulin-like lectin 9 (Siglec-9) has been discovered to be a granulocyte ligand for VAP-1. Binding between Siglec-9 and VAP-1 was confirmed by *in vitro* and *ex vivo* adhesion assays [13]. When Siglec-9 motif containing peptide was labeled with ^{68}Ga and used as a PET tracer, VAP-1 on vasculature was detected at sites of inflammation and cancer [13-15].

We hypothesized that PET-CT with a [^{68}Ga]Ga-DOTA-Siglec-9 tracer would allow quantification of regional pulmonary inflammation. The aim of the study was to examine this hypothesis in a porcine model of ARDS [16]. The location and magnitude of early inflammatory changes were investigated using PET-CT imaging with [^{68}Ga]Ga-DOTA-Siglec-9. In addition, the tissue perfusion was assessed using [^{15}O]water PET-CT. The findings were correlated with histological and immunohistochemical information. Healthy animals were studied as controls.

Material and methods

Tracer production and quality control

Sodium acetate buffer (pH 4.6), sodium hydroxide (10 M), and doubly distilled hydrochloric acid (Riedel de Haën) were obtained from Sigma-Aldrich Sweden (Stockholm, Sweden). Trifluoroacetic acid (TFA) was obtained from Merck (Darmstadt, Germany). The purchased chemicals were used without further purification. The precursor ligand comprising 1,4,7,10-tetraaza cyclododecane-1,4,7-tris-acetic acid chelator moiety conjugated via ethylene glycol with disulfide-bridged CARLSL-SWRGLTLCPSK peptide (DOTA-Siglec-9; custom synthesis from Peptide Specialty Laboratories GmbH, Heidelberg, Germany) [13] was dissolved in deionized water to give 1 mM solution.

^{68}Ga ($t_{1/2}$ = 68 min, β^+ = 89%, and electron capture of 11%) was eluted with 0.1 M HCl from two tandem ^{68}Ge/^{68}Ga-generators [17] (1850 MBq, Eckert & Ziegler, Berlin, Germany), where ^{68}Ge ($t_{1/2}$ = 270.8 d) was attached to a column of an inorganic matrix based on tin dioxide. The production and quality control of the tracer was accomplished within one hour. The generator eluate fractionation method was used for the labeling [18]. The first ^{68}Ga eluate fraction of 1.5 mL was sent to the waste and the next 1.0 mL containing over 65% of the total radioactivity was collected and buffered with 200 µL of acetate buffer and 10 µL of sodium hydroxide to provide pH of 4.6±0.4. Hundred µl of 99.5% ethanol was added in order to exclude possible radiolysis due to the presence of oxidation sensitive amino acid residues. Ten nanomoles of DOTA-Siglec-9 was added and the reaction mixture was heated at 75°C for 15 min.

The crude product was analyzed by high-performance liquid chromatography (HPLC) on Elite LaChrom system (Hitachi, VWR) consisting of an L-2130 pump, UV detector (L-2400), and a radiation flow detector (Bioscan) coupled in series. Separation of the analytes was accomplished using endcapped analytical column with stationary phase of covalently bonded pentylsilane (Discovery BIO Wide Pore C5; 5cm×4.6 mm). The conditions for the HPLC analysis were as follows: A = 10 mM TFA; B = 70% acetonitrile, 30% H_2O, 10 mM TFA with UV-detection at 220 nm; linear gradient elution: 0-2 min at 35% B, 2-9 min at 35 to 100% B, 9-12 min at 100% B; flow rate was 2.0 mL/min. Data acquisition and handling were performed using the EZChrom Elite Software Package. The recovery of the radioactivity from the HPLC column was determined performing analysis with and without the column and collecting the frac-

tions for the subsequent measurement of the radioactivity in a well-type NaI(Tl) scintillation counter (Uppsala Imanet AB, GE Healthcare, Uppsala, Sweden) with correction for dead-time and decay. The resulting product was formulated with sterile phosphate buffer (pH 7.4) and used without further purification since the buffer was biologically compatible and the radiochemical purity was over 95% with individual impurities less than 5%.

Animal investigational protocol and instrumentation

The animal ethics committee in Uppsala, Sweden approved the study and the animals were treated in accordance with the European Union directive. We studied four pigs (weighing on average 27.5 kg (range 24.7-27.7 kg)) of mixed Hampshire, Yorkshire, and Norwegian country breeds. All animals, lying in the supine position, received intravenous (i.v.) anesthesia using a combination of fentanyl, ketamine, and midazolam. Adequate depth of anesthesia was ascertained by no reaction from pain stimulation between the front hoofs. The animals were tracheotomized and instrumented, and then paralyzed with pancuronium. The depth of anesthesia was then monitored continuously by observing arterial blood pressure and heart rate. After instrumentation, a period of 15 min was allowed for stabilization. One control pig was anesthetized and euthanized immediately, without any other invasive procedure.

The trachea was intubated with a cuffed endotracheal tube and secured in place, and the lungs were mechanically ventilated by a Servoi (Maquet Critical Care, Solna, Sweden). Baseline ventilation was delivered in volume-controlled mode with a tidal volume (VT) of 6-8 mL/kg, respiratory rate (RR) of 30 bpm, positive end-expiratory pressure (PEEP) of 5 cm H_2O, inspiratory to expiratory ratio (I:E) of 1:2, and inspired oxygen fraction (F_IO_2) of 0.35. Standard monitoring included electrocardiography, invasive arterial, central venous, and pulmonary pressure at baseline and post two-hit ARDS model as previously described [19]. The end-inspiratory and end-expiratory pressures obtained during three second pauses were used for calculating respiratory mechanics. A cystostomy was performed through a midline mini-laparotomy for the measurement of urine output. Gas exchange was measured using conventional blood gas analysis (Radiometer ABL 505; Radiometer OSM3) and derived parameters were calculated according to the standard formula.

Lung inflammation (ARDS) model and mechanical ventilation

The two healthy control animals were instrumented, subjected to a 10 minute period of stabilization and then immediately transferred to the PET-CT facilities. In the other two animals an acute lung inflammatory process was induced by repeated lung lavages of warmed isotonic saline (30 mL/kg) applied until PaO_2/F_IO_2 less than 200 mmHg was reached followed by 120 minutes of injurious mechanical ventilation using low PEEP (mean PEEP = 2 cm H_2O), high inspiratory pressures (mean plateau pressure = 36 cm H_2O), RR 20, and I:E 1:2. This method has been shown to induce severe lung injury and inflammation, similar to human ARDS as indicated by [^{18}F]FDG-PET and inflammatory markers [16, 20]. At the end of this period, we recorded a new set of physiological data. After the inflammatory lung model was established, we set the ventilator on pressure controlled ventilation with an inspiratory pressure of 25 cm H_2O, PEEP of 5 cm H_2O, inspiratory time of 0.5 s, respiratoryrate of 25 bpm and F_IO_2 of 1.0. These settings were maintained until the end of the study. Ringer's acetate was given i.v. at a rate of 30 mL/kg/h during the instrumentation, 20 mL/kg/h during the lung injury induction, and 10 mL/kg/h until the end of the protocol.

In vivo PET-CT examinations

The anesthetized pigs were positioned in the center of the 15 cm axial field of view of a Discovery ST16 PET-CT scanner (General Electric Medical Systems, USA; 15.7-cm axial and 70-cm trans-axial field of view) in order to include the thorax with apical-caudal distance of the lungs. The positioning was performed using low dose CT scout view (140 kV, 10 mAs). Attenuation correction and anatomical reference for PET was acquired by a 140 kV, 10-80 mA CT examination.

The PET examinations were started with a 10-min dynamic scan (26 time frames; 1×10, 8×5, 4×10, 2×15, 3×20, 2×30, 6×60 s) and simultaneous intravenous bolus administration of 421±4 MBq [^{15}O]water in order to assess

lung tissue perfusion. Then, [^{68}Ga]Ga-DOTA-Siglec-9 (120±36 MBq, 22±2 μg peptide) was intravenously administered and the pigs were examined by a dynamic PET protocol for 90 min (33 frames; 12×10, 6×30, 5×120, 5×300, 5×600 s) over the same position followed by whole-body scanning with 3 min per bed position (5 partly overlapping bed positions). Attenuation correction and morphological CT were obtained in the same way as for the dynamic scan.

Acquired PET data were reconstructed using normalization and attenuation-weighted ordered subsets expectation maximization algorithm (2 iterations, 21 subsets) including corrections for dead time, random coincidences as estimated by singles count rates, model-based scatter correction [21], attenuation correction based on a bilinear conversion of Hounsfield units to 511 keV attenuation coefficients, and decay. A 5.4 mm Gaussian post-filter was applied. Reconstructed images were analyzed using VOIager 4.0.7 software (GE Healthcare, Sweden). Regions of interest (ROIs) were delineated on trans-axial CT slices. Entire organs were delineated on sequential slices and combined into volumes of interest (VOIs). In addition, VOIs were defined over the left and right ventricle of the heart in the PET images to define input functions for kinetic modeling. Lung CT VOIs were transferred to the [^{15}O]water examination to assess tissue perfusion in the entire lung. Standardized uptake value (SUV) normalized to body mass and injected amount of radioactivity were determined using the mean radioactivity concentration in VOIs (SUV = (organ radioactivity/organ weight)/(total given radioactivity/body weight)). In the case of [^{68}Ga]Ga-DOTA-Siglec-9 the last 25 min of the dynamic PET data were summed over time to create average images. VOIs were projected onto each individual frame to create organ time-(radio) activity curves (TACs).

During [^{68}Ga]Ga-DOTA-Siglec-9 PET arterial blood samples (1 mL) were collected at 0.5, 1, 2, 5, 7, 10, 15, 20, 30, 45, 60, 75, 80 and 90 min post injection in order to measure the radioactivity concentration in whole blood and plasma for the subsequent blood clearance calculation and kinetic modeling. Accurate cross-calibration between PET-CT, dose calibrator and well counters used to measure blood radioactivity was verified on a monthly basis and was always within 3%.

Kinetic analysis

Lung tissue perfusion was quantified from dynamic [^{15}O]water PET data, using either right and left ventricle TAC as input functions. The data was fit to a single tissue compartment model with blood volume parameter using non-linear regression in in-house developed software in MATLAB.

The dynamic [^{68}Ga]Ga-DOTA-Siglec-9 PET data from the lung was fitted to a reversible two-tissue compartment model with blood volume parameter (Equation 1) using non-linear regression. The model consists of three components each of which is a function of time and is obtained from the experimental TACs. Input function, C_{plasma} (C_p) consists of the arterial blood and the interstitial space close to vessels. The irreversible model contains K_1, k_2, k_3 kinetic parameters, while the reversible model contains K_1, k_2, k_3, and k_4 kinetic parameters. Tracer radioactivity concentration in plasma used as input function was obtained by multiplication of the left-ventricle TAC with the mean plasma-to-whole blood ratio of the measured arterial blood samples. The output parameter, total volume of distribution (V_T), defined as the ratio of K_1/k_2, was used to assess changes in tracer uptake and differences between healthy and injured animals. Net uptake rate ($k_i = K_1*k_3/(k_2+k_3)$) of [^{68}Ga]Ga-DOTA-Siglec-9 was calculated as the slope of the linear portion of the plot, starting at 15 min post injection. The values were corrected for free fraction of tracer in plasma calculated based on plasma protein bound [^{68}Ga]Ga-DOTA-Siglec-9 as described below.

$$\frac{dC_1(t)}{dt} = K_1 C_p(t) - (k_2 + k_3) C_1(t) + k_4 C_2(t)$$

Equation (1), where, C_p is concentration of the radioactivity in the plasma; C_1 is free and non-specifically bound tracer in tissue; and C_2 is specifically bound tracer.

Plasma protein binding

Arterial blood samples (1 mL, in tubes with sodium heparin) collected at 5 and 80 min time points were centrifuged at 3,000×g for 4 min at +4°C. The plasma was separated, weighed, and radioactivity was measured in a well-type NaI(Tl) scintillation counter. Then plasma was transferred (3×200 μL) into micro centrifuge filters (Costar®, Spin-X, Sigma) and the radioac-

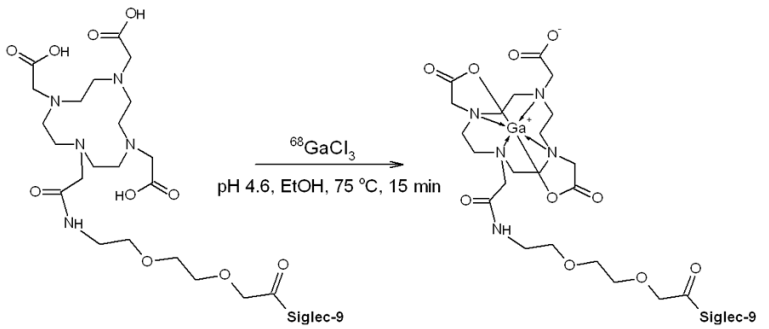

Figure 1. Schematic representation of [^{68}Ga]Ga-DOTA-Siglec-9 production, where Siglec-9 represents the cyclic peptide with amino acid sequence of CARLSLSWRGLTLCPSK, i.e. consisting residues 283 to 297 from Siglec-9. The ligand has 8-amino-3,6-diooxaoctanoyl linker (polyethylene glycol derivative) between the chelator moiety and the peptide.

tivity of each tube was recorded. For the compensation of potential losses of the radioligand adsorbed to plastic surfaces or filter membranes, 10 µL of tracer was mixed with a buffer (190 µL 50 mM Tris-HCl, pH 7.4) equal to the volume of plasma and used as described above. The filters were centrifuged at 20,800×g for 12 min at +4°C. Thereafter the radioactivity of the filter and filtrate was measured. The radioactivity of the original plasma samples (50 µL, in triplicate) was measured for the reference. The fraction of the free tracer in plasma was defined as the ratio between radioactivity in the filtrate and that in plasma, divided by the ratio between radioactivity in the filtrate and that in the buffer.

Post-mortem tissue sampling and assays

The animals were euthanized by intravenous injection of potassium chloride under deep anesthesia after the [^{68}Ga]Ga-DOTA-Siglec-9 PET-CT scanning and subsequent infusion of monoclonal anti-human VAP-1 antibody (1B2). The ventilation was maintained unchanged and the thoracic cage was opened by a sternotomy. The mechanical ventilation was discontinued. Thereafter the trachea was clamped at the carinal level, and the heart and lungs were excised. The organs were taken out in one piece and tissue samples from apical, medial, and caudal areas of the lungs as well as skeletal muscle, liver and heart were harvested, immediately transferred into cryovials, and shock frozen in order to avoid protein degradation. Two sets of samples were collected for the radioactivity biodistribution assessment and immunohistochemistry assay of VAP-1 receptors.

For tissue radioactivity distribution assessment, the harvested samples were weighed and the radioactivity was measured using a well-type NaI(Tl) scintillation counter and decay-corrected to the time of injection. The results were expressed as SUV.

For the post-mortem assessment of VAP-1 receptor expression, 18 mL (0.84 mg/mL) of 1B2, recognizing porcine VAP-1 [22] was infused at a constant 3.3 mL/min rate during 5 min after the PET scanning. The tissue samples were stored in cryovials (1.8 mL) suitable for liquid nitrogen and long-term storage at -70°C. The immunohistochemical assessment of the presence of VAP-1 receptors was performed on 5 µm acetone fixed frozen sections stained either only with the second stage antibody, fluorescein isothiocyanate (FITC)-conjugated-anti-mouse IgM, or with 1B2 followed by the second stage antibody, FITC-anti-mouse IgM.

Another set of samples was immersed in 10% buffered formalin and later embedded in paraffin, cut into slices of 4 µm thickness, and stained with hematoxylin-eosin for histological analysis. A pathologist blinded to the experimental origin of the specimens assessed the histology. A quantitative morphometric analysis of alveolar collapse, emphysema, alveolar edema, alveolar and septal leukocytes, perivascular and peribronchial leukocytes, and interlobular and septal edema and leukocyte infiltration were assessed. Each item was scored 0-4+ depending on severity (0 = not observed; + = mild; ++ = moderate; +++ = severe; and ++++ = very severe).

Statistical analyses

Statistical analysis was conducted with GraphPad Prism software (version 5.00, Graph Pad Software Inc, La Jolla, CA, USA). Non-linear regression analysis was also performed with GraphPad Prism software and the goodness of fit to the variables was presented as R^2 values.

Table 1. Physiological characteristics of the study animals

	Ventilated controls		ARDS animal 1		ARDS animal 2	
	Animal 1	Animal 2	preVILI*	postVILI*	preVILI*	postVILI*
Pplateau, cm H_2O	11	13	16	25	18	24
PaO_2/F_IO_2, mmHg	540	532	517	145	471	214
*p*CO2, mmHg	37	47	41	44	43	59
Shunt, %	12	12	13	44	16	22
RS Compliance, mL/cm H_2O	29	33	20.9	10.7	23	13
Cardiac output (CO), l/min	2.84	3.73	2.64	3.33	2.64	3.84

*VILI: Ventilation induced lung injury.

Table 2. Histological score from non-ventilated and ventilated healthy controls and ARDS animals

Healthy non-ventilated control			
Left lung region	Grade	Right lung region	Grade
Apical	+	Apical	+
Middle	+	Middle	++
Caudal	+	Caudal	++
Healthy ventilated control			
Left lung region	Grade	Right lung region	Grade
Apical	+++	Apical	+++
Middle	+	Middle	+
Caudal	+	Caudal	++
ARDS animals			
Left lung region	Grade	Right lung region	Grade
Apical	++++	Apical	+++
Middle	++++	Middle	++++
Caudal	++++	Caudal	++++

Data are given as mean ± SD when relevant. The statistical significance of differences between the data sets was determined by Wilcoxon matched pairs test and Mann-Whitney test. A *P* value below 0.05 was considered statistically significant.

Although the number of animals in this study was limited, the consistency of the results was high and clearly seen in terms of respiratory mechanics, oxygenation goals, histological and immunohistological findings as well as PET-CT imaging and kinetics. Due to the high consistency of the results, ethical considerations discouraged us from increasing the number of animals that would be sacrificed unnecessarily in the experiment. Moreover, statistical investigations demonstrated that if the within-pair correlation is high then a paired *t-test* is feasible even with as extremely small *N*s as two [23].

Results

Radiochemistry

Two tandem $^{68}Ge/^{68}Ga$ generators were used in order to increase the radioactivity amount. The radioactivity incorporation was over 95% with radiochemical yield of 70±5% and specific radioactivity of 25±2 MBq/nmol (n = 4). The product purification was omitted due to the high radioactivity incorporation and consequently radiochemical purity higher than 95%. Ten percent (volume) of ethanol was added to the reaction mixture in order to suppress possible radiolysis due to the oxidation sensitive tryptophan (**Figure 1**).

Animal study

No differences in baseline data of hemodynamic or respiratory mechanics could be observed (**Table 1**). All animals survived until the end of the experiments. The time from the anesthesia induction until the image acquisition was 1 and 5 h, respectively for healthy and injured animals. The total time of the mechanical ventilation from the anesthesia induction until the euthanasia was 4.5 and 9 h, respectively for healthy and injured animals. The ARDS and healthy pigs had mean arterial blood pressure (MAP) values ranging, respectively between 99 to 100 mmHg and 76 to 91 mmHg at the time of the scans.

Histological analysis

Histological analysis was performed on the ARDS and healthy ventilated controls after PET scanning as well as on the non-ventilated animal. At macroscopic evaluation the ARDS animals had red, brilliant and heavy lungs, while the healthy animals had pink and light lungs.

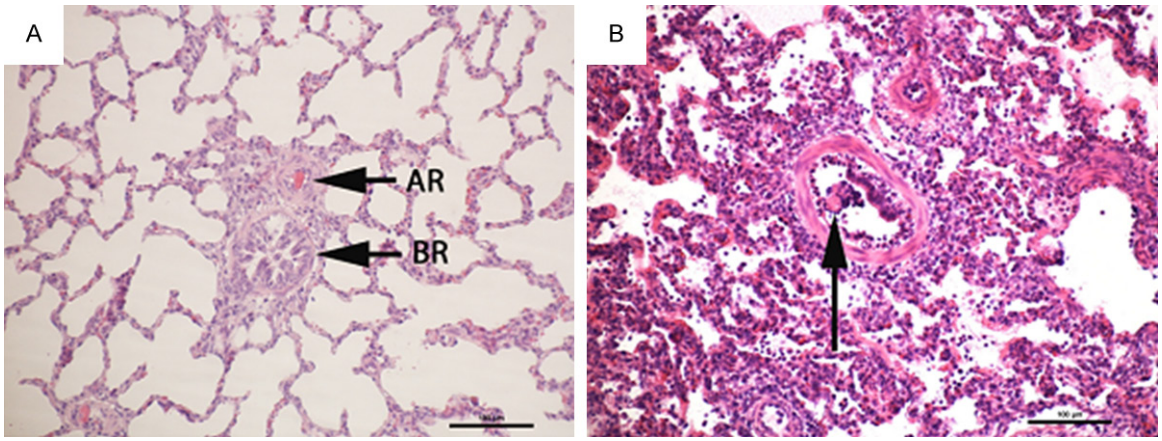

Figure 2. Representative hematoxylin-eosin staining from healthy ventilated control (A) and ARDS (B) animals from caudal region of the lung. (A) Seemingly normal lung parenchyma with low number of diffused leukocytes. In the center of the picture bronchial (BR) and arteriolar lumen (AR) are visible. (B) Acute inflammation in the lung. Alveoli, peribronchial and perivascular areas show infiltrated leukocytes. Notice in the center of the picture a bronchial lumen, containing cast of cells, necrotic cells, and fibrin (arrow). The scale bars correspond to 100 μm.

Both groups had limited areas of collapse in dependent lung regions. The animal which did not undergo mechanical ventilation had pink and light lungswithout any dependent lung collapse. The lungs from the ARDS animals had substantially higher inflammation score (patchy lobular inflammation, and diffuse alveolar collapse with inflammation), as well as thickened alveolar septum, stasis of leukocytes and septal and alveolar edema with a score of 4+ in both pigs and with no difference between apical, middle, and caudal regions (**Table 2** and **Figure 2**). The lungs of the healthy, ventilated controls had a lower inflammation score (incipient, focal peribronchial, perivascular and alveolar inflammation) with the value of 1+ in the middle and caudal regions and value of 3+ in apical region. The histological findings in the lungs from non-ventilated animal were similar to those in the healthy ventilated animals, except for only a moderate inflammation in the apical region and the score was 1+ in all lung regions.

Organ distribution and TACs of [^{68}Ga]Ga-DOTA-Siglec-9

The amount of the administered peptide mass and radioactivity was kept similar in all experiments with [^{68}Ga]Ga-DOTA-Siglec-9 (22±2 μg; 120±36 MBq). The whole-body biodistribution of [^{68}Ga]Ga-DOTA-Siglec-9 showed significant uptake in lung, kidneys and urinary bladder for both ARDS and healthy ventilated animals (**Figure 3**). Uptake in kidneys and urinary bladder was presumably due to the excretion.

The uptake of [^{68}Ga]Ga-DOTA-Siglec-9 in other organs such as liver, heart, and muscle, was negligible in both healthy and ARDS pigs. The plasma kinetics of the tracer was determined during 90 min of dynamic scanning demonstrating rapid blood clearance of radioactivity for both healthy and ARDS animals, respectively with only 1.3% and 0.9% (healthy ventilated animals) and 2.5% and 1.3% (ARDS animals) of remaining radioactivity at 90 min. These data correlated well with the results obtained from the arterial blood sampling at 0.5, 1, 2, 5, 7, 10, 15, 20, 30, 45, 60, 75, 80 and 90 min post injection. The fraction of the blood radioactivity concentration associated with the plasma was stable within 90 min and was similar for the healthy and ARDS animals with values of 71.4±2.0% and 72.6±1.5%, respectively. Rapid washout pattern was observed from most of the organs except for kidneys. The background uptake was marginally higher for the injured animals.

The blood clearance kinetics was best described by a bi-exponential function with slow and fast phases of half-life values of 11.3/0.6 and 5.4/0.3 min (R^2 = 0.9955 and 0.9990), respectively for the two healthy animals (HP1 and HP2) and 10.2/0.7 and 7.8/0.5 min (R^2 = 0.9844 and 0.9876), respectively for the two ARDS animals (**Figure 5A**). The binding of [^{68}Ga]Ga-DOTA-Siglec-9 to the plasma pro-

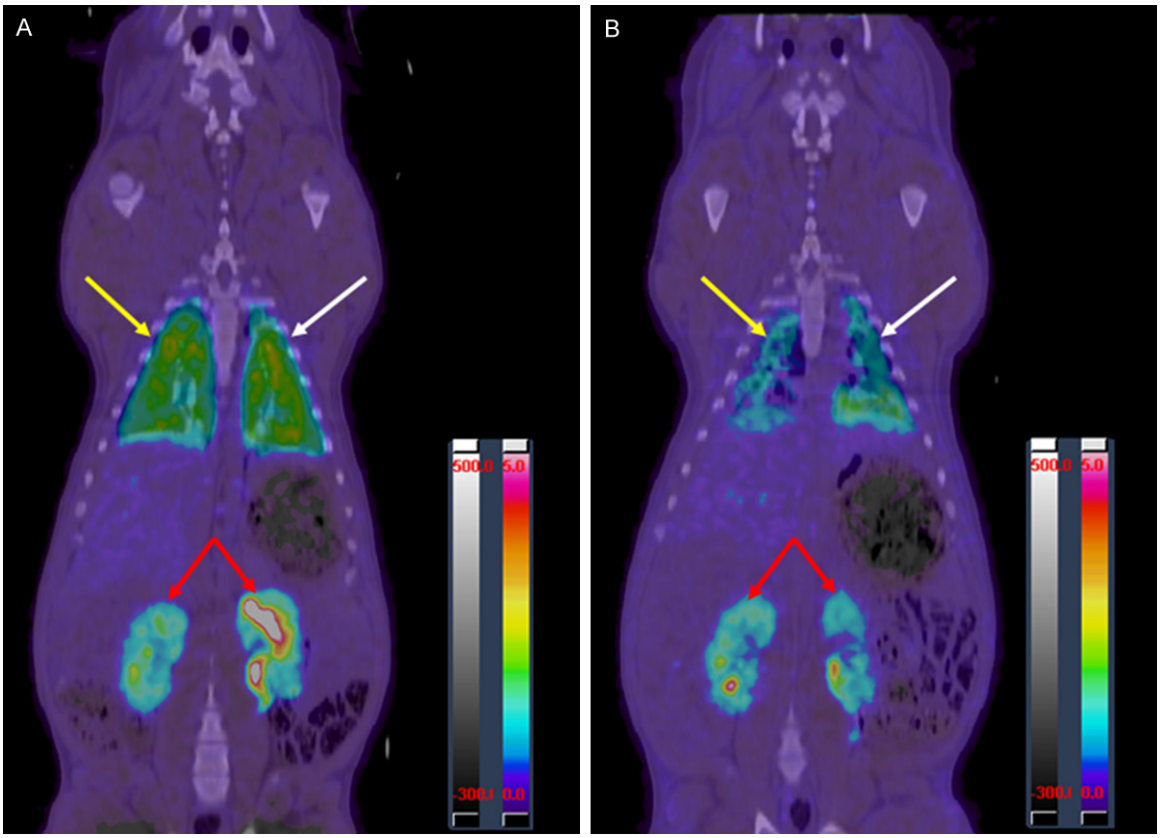

Figure 3. Whole-body distribution of i.v. injected [^{68}Ga]Ga-DOTA-Siglec-9 presented as coronal section of fused PET-CT images at 120 min post injection. A. Healthy ventilated animal; B. ARDS animal. Yellow and white arrows point, respectively, at radioactivity signal in the right and left lung. Red arrows point at kidney radioactivity signal. The images are displayed in the same color scale. Grey and colored scale bars correspond, respectively to CT and PET images.

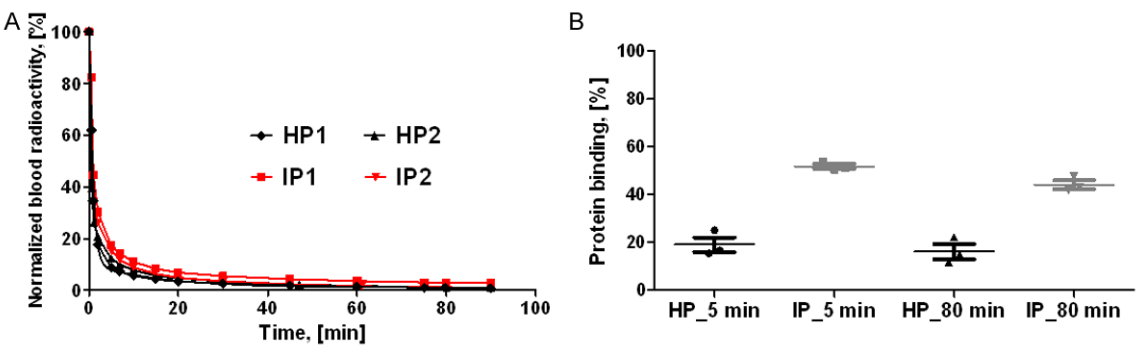

Figure 4. A. Blood clearance kinetics of [^{68}Ga]Ga-DOTA-Siglec-9 obtained from the blood sampling data (R^2 = 0.9955, 0.9990, 0.9844 and 0.9876). HP1: healthy ventilated animal number 1; HP2: healthy ventilated animal number 2; IP1: ARDS animal number 1; IP2: ARDS animal number 2; B. Plasma protein binding of i.v. injected ^{68}Ga-DOTA-Siglec-9 (blood sampling at 5 and 80 min time point; triplicates; 2 animals/group).

teins was measured at 5 min and 80 min post administration (**Figure 4B**). There was no statistically significant difference in the binding extent between the two time points. The protein binding was higher in the ARDS animals than in controls and it was reflected in the longer blood circulation of the tracer and the marginally higher background uptake. The free fraction of tracer in plasma was taken into account in the kinetic modeling.

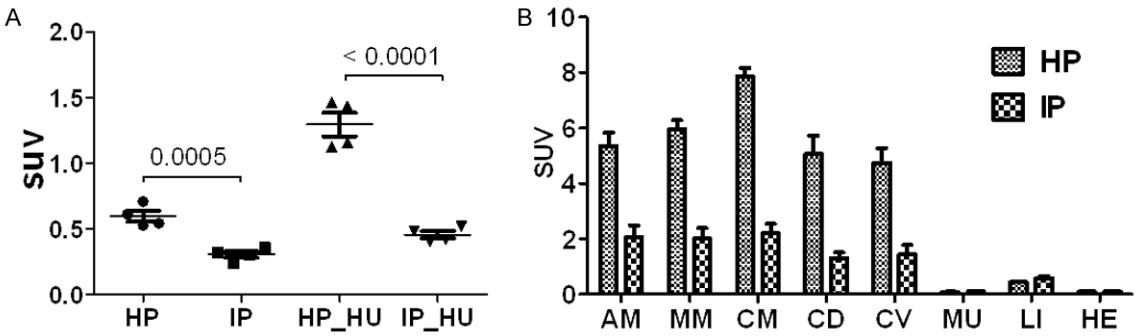

Figure 5. A. SUVs of ^{68}Ga-DOTA-Siglec-9 imaging obtained from whole-body scanning and corrected for the lung density using Hounsfield Units (HU) from the corresponding CT images. Mean ± SD (n = 4 lungs). HP: four lungs of the healthy animals without correction for tissue density; HP_HU: four lungs of the healthy animals with correction for tissue density; IP: four lungs of the ARDS animals without correction for tissue density; IP_HU: four lungs of the injured pigs with correction for tissue density; B. Tissue sample radioactivity distribution presented as decay-corrected SUV values. AM: apical medial; MM: medial medial; CM: caudal medial; CD: caudal dorsal; CV: caudal ventral are lung regions from where the tissue was collected. MU: muscle; LI: liver; HE: heart. The data is presented as mean ± SD (n = 6, sampled tissue).

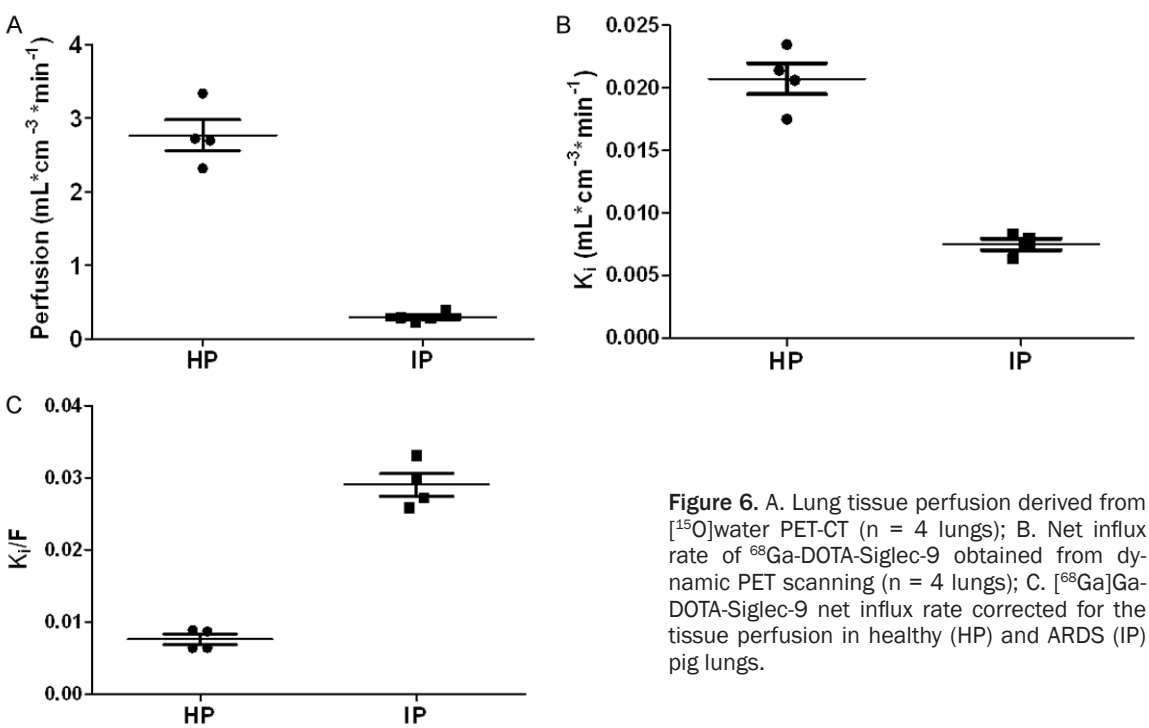

Figure 6. A. Lung tissue perfusion derived from [^{15}O]water PET-CT (n = 4 lungs); B. Net influx rate of ^{68}Ga-DOTA-Siglec-9 obtained from dynamic PET scanning (n = 4 lungs); C. [^{68}Ga]Ga-DOTA-Siglec-9 net influx rate corrected for the tissue perfusion in healthy (HP) and ARDS (IP) pig lungs.

The *in vivo* distribution was determined in lung, heart, liver and muscle from the dynamic scanning images at 85 min, and presented as SUV values. The correction for the lung density increased the SUVs, however the relation between the healthy and ARDS animals remained similar (**Figure 5A**). There was statistically significant difference between the lungs from healthy (n = 4 lungs) and ARDS (n = 4 lungs) animals without (P = 0.0005) and with (P<0.0001) correction for the tissue density using Hounsfield Units. The uptake of [^{68}Ga]Ga-DOTA-Siglec-9 was higher in all lung regions for the healthy animals. However, it was lower in liver, heart right ventricle and muscle. These results correlated well with the *ex vivo* distribution data (**Figure 5B**) where the SUV was calculated by measuring the radioactivity concentra-

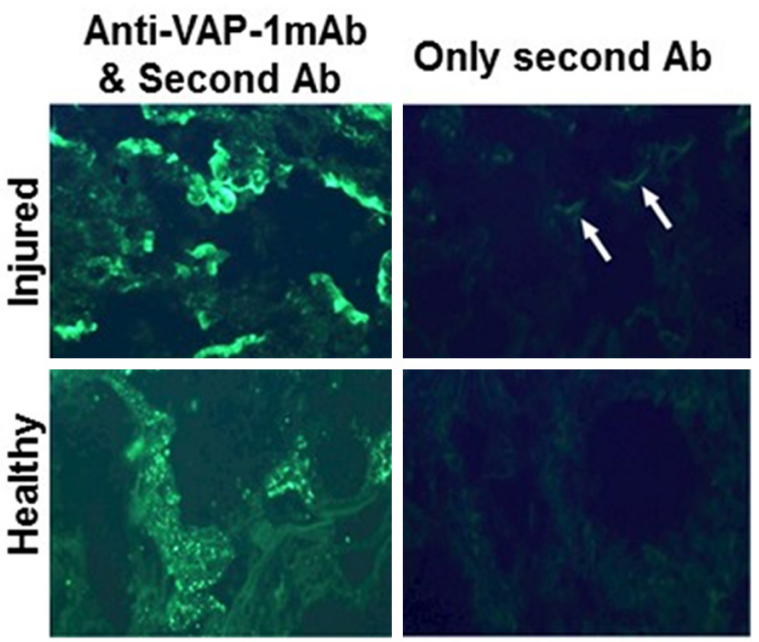

Figure 7. VAP-1 was differentially located in the lungs of ARDS and healthy pigs. The upper panel shows the positivity in the ARDS lung tissue and the lower panel depicts the healthy pig lung tissue. 1B2: monoclonal anti-VAP-1 antibody; Second Ab: fluorescein isothiocyanate conjugated anti-mouse IgM.

tion in the post-mortem tissue samples collected from various lung regions.

Kinetic analysis

In the healthy pigs, the kinetics of [^{15}O]-water was described accurately using the right ventricular TAC as input function, whereas in the injured pigs, the perfusion was described using the left ventricular TAC as input function. Using the alternative ventricle resulted in visually poor fits in both cases. The tissue perfusion (F) in the injured lungs (2.8±0.4, n = 4) was decreased by factor of 10 (P<0.0001) compared to the healthy animal lungs (0.3±0.1, n = 4) (**Figure 6A**).

The two-tissue compartment model described the [^{68}Ga]Ga-DOTA-Siglec-9 TACs well. A significant difference (P<0.001) was found for the net uptake rate (K_i) of [^{68}Ga]Ga-DOTA-Siglec-9 with values of 0.026±0.003 and 0.014±0.002 mL/g/min, respectively for healthy and ARDS pigs (**Figure 6B**). The net uptake rate (K_i) of [^{68}Ga]Ga-DOTA-Siglec-9 was about 55% lower in ARDS pigs as compared with healthy pigs. However, correction of K_i for the tracer delivery to the target, i.e. normalizing K_i for total tissue perfusion (K_i/F) resulted in the 4-fold enhancement in the ARDS pigs (**Figure 6C**). The retention (K_i/K_1) of [^{68}Ga]Ga-DOTA-Siglec-9 in the lung was also higher for the ARDS pigs (0.17±0.01, n = 4 lungs) than for the healthy ventilated pigs 0.12±0.02 (n = 4 lungs) with P = 0.0017.

Post-mortem assessment of VAP-1 receptors

After the PET-CT examination the animals were i.v. administered with anti-VAP-1 antibody for the post-mortem immunohistochemistry assessment of the presence of luminal VAP-1 receptors. VAP-1 was distributed in endothelial cells differently in the healthy and ARDS pigs . In the stainings with anti-VAP-1 antibody (1B2) followed by the second stage antibody, the positive signal in ARDS lungs was located near to the endothelial cell surface, whereas in healthy pigs, VAP-1 was still stored within the endothelial cell granules (**Figure 7**, left panel). However, very little of the injected first stage anti-VAP-1 antibody was detected on the surface even in the ARDS lungs and practically nothing in healthy lungs, when only the second stage was employed.

Discussion

To our best knowledge this is the first attempt to evaluate lung inflammation in a porcine ARDS model using VAP-1 targeting [^{68}Ga]Ga-DOTA-Siglec-9 as a PET tracer. The inflammation detection was feasible, however it required additional procedures including kinetic modeling and perfusion data obtained from [^{15}O]water PET.

Previously, [^{18}F]FDG PET-CT has demonstrated the feasibility of monitoring the temporal and spatial evolution of lung inflammation [16, 24-26]. However, [^{18}F]FDG uptake in the inflammatory tissue is a non-specific reflection of an increased metabolic state and mainly the activation of inflammatory cells. An imaging agent with a specific uptake mechanism that would allow quantitative characterization of the

inflammation in stationary cells is of considerable interest. This approach may open new opportunities for diagnosing, better understanding of pathophysiology and underlying injury mechanisms, therapy planning and monitoring of the treatment efficacy, as well as for drug development.

[^{68}Ga]Ga-DOTA-Siglec-9 was developed as a ligand to VAP-1 receptor, which was demonstrated to translocate from the intracellular storage granules to the endothelial cell surface by inflammatory stimuli. Salmi and coworkers [27] reported constitutive expression of VAP-1 in the human endothelium from liver, kidney and peripheral lymph nodes, and also in smooth muscle cells of large vessels, and this expression was up-regulated during inflammation. Moreover, Jaakkola and coworkers, demonstrated that VAP-1 was present in porcine lung endothelium [22]. They also reported that VAP-1 was translocated to capillary endothelial surface of skin and joints by inflammatory stimuli such as chemical dermatitis and arthritis. In addition, they found that the distribution of VAP-1 was similar in pigs and humans, including the pulmonary vascular bed [22]. Later, Singh and coworkers [28] reported that VAP-1 expression in lungs was restricted to the endothelial and smooth muscle cells of pulmonary arteries and veins of normal and inflamed murine lungs, and of normal human lungs. All these assessments were done by immunohistochemistry of post-mortem histological preparation using a primary antibody against VAP-1. However, this assessment gives information related to the protein expression but not to its location or functionality. In our study the anti-VAP-1 antibody was administered *in vivo* allowing assessment of VAP-1 location and expression in the living organism. Then the subsequent *in vitro* assay using a secondary antibody revealed the distribution of VAP-1 proteins on the surface of the endothelium and inside the cells.

The porcine model of ARDS used in this study previously demonstrated higher uptake of [^{18}F] FDG in inflamed lungs as compared to healthy ones [16]. The early inflammation was localized preferably in gravitational intermediate regions. The model resulted in heterogeneously aerated lungs with significant amount of non-aerated and hyper-inflated tissue as well as tidal recruitment and hyperinflation [16]. In addition, worse respiratory system compliance and oxygenation as well as higher inflammatory histological score were observed in the ARDS lungs. In order to allow adequate time for developing inflammation and translocation of VAP-1 onto the endothelial surface [29], we scheduled the [^{68}Ga]Ga-DOTA-Siglec-9 PET-CT examination four hours post ARDS induction. The histological analysis showed significantly higher inflammation in lungs from ARDS animals as compared with healthy controls also in this study. Importantly, the inflammatory score from the healthy non-ventilated animal and healthy ventilated controls was very similar. These findings suggest that the used protective mechanical ventilation successfully prevented lung inflammation in the ventilated control group during the time of PET-CT acquisition.

The feasibility of the noninvasive *in vivo* visualization of inflammation using prototypic ^{68}Ga-labeled ligand (^{68}Ga-DOTAVAP-P1) against VAP-1 has been demonstrated in extra-pulmonary inflammation models, and the discrimination of bone infection from aseptic inflammation was possible in experimental models of osteomyelitis [8]. The present study is the first one to investigate the *in vivo* targeting of VAP-1 in lung inflammation using Siglec-9 based tracer, which in previous studies has shown good inflammation imaging results in other inflammatory animal models [13] and has demonstrated high *in vitro* stability [15]. In this study, the assessment of the feasibility of lung inflammation detection by [^{68}Ga]Ga-DOTA-Siglec-9 PET-CT was conducted in a porcine ARDS model by mechanically induced lung injury and subsequent inflammation. Healthy animals were used for the baseline comparison. It is worth mentioning that a slight degree of inflammation was revealed by histology analysis even in the early control animal that was not mechanically ventilated. The results were comparable to those of healthy ventilated animals indicating that minor inflammation may occur naturally in farm-bred pigs. Studying lung inflammation in this model was complicated by the presence of high physiological expression of VAP-1 in the healthy porcine lungs. This is however not restricted to this model since it has also been demonstrated in rat experiments where the uptake of ^{68}Ga-DOTAVAP-P1 in healthy rat lungs was even higher than in the sites of sterile inflammation

in the neck [9]. In the present study, the biodistribution of [^{68}Ga]Ga-DOTA-Siglec-9 was dominated by lung and kidney followed by liver and heart. The blood clearance was rapid in both healthy and ARDS animals. The higher lung SUV as compared to blood SUV at later time points also indicated retention. The lung SUVs were higher in healthy animals compared to ARDS animals in all lung regions. However, the location of VAP-1 on the endothelial cell surface as determined by immunohistochemistry was different in the ARDS and healthy animals. The presence of VAP-1 on the luminal face of the endothelium cellular membrane was higher in ARDS lungs than in healthy ones, although still rather minimal for example in comparison to the skin inflammation in patients [30]. The healthy controls presented cytoplasmic VAP-1 granules in contrast to the ARDS animals that presented a higher signal in the peri-membrane position. These results suggest that VAP-1 was absent on the luminal endothelial surface of the healthy animals and was translocated from intracellular granules to the membrane secondary to lung inflammation in ARDS animals.

Another point to remark is the slightly higher background radioactivity found in the ARDS animals. Biotrauma is caused by a complex array of inflammatory mediators, resulting in a local and systemic inflammatory response propagating injury to non-pulmonary organs, which may result in multiple system organ dysfunctions, and ultimately in death [31]. It is probable that secondary to biotrauma, extrapulmonary tissues could have activated the endothelium and expressed VAP-1 in an extrapulmonary position resulting in an increase of background uptake. Also, in some inflammatory conditions (e.g. in atherosclerosis, psoriasis, diabetic retinopathy) the amount of soluble VAP-1/semicarbazide-sensitive amine oxidase (SSAO) is increased in plasma [32-34]. The slightly increased background/muscle radioactivity concentration in the ARDS animals and higher plasma protein binding may indicate that the integrity of the endothelium was compromised and the VAP1 was released into the blood stream where [^{68}Ga]Ga-DOTA-Siglec-9 could bind to soluble VAP-1 in plasma.

The role of the tissue perfusion and thus [^{68}Ga]Ga-DOTA-Siglec-9 accessibility to the tissue was assessed by performing PET-CT with [^{15}O]water. The kinetic modeling of [^{15}O]water separates extravascular tissue fluid flux from the intravascular water content. Remarkably, the tissue perfusion was lower by a factor of ten in the ARDS lungs, while intravascular blood flow, largely defined by cardiac output, was unchanged. This might depend on the inflow of water from the vascular bed to the extracellular space and the return of fluid back to circulation via capillaries, venules and lymph vessels. Moreover, the turnover can also depend on the amount of edema: the larger the extravascular water pool (as in edema), the less is the turnover of water per tissue volume [35]. Interestingly, the [^{15}O]water data could only be fitted using the left-ventricular TAC as input function in the injured animals, whereas it was fitted best using the right-ventricular input curve in the healthy animals. This would indicate that the lung tissue was primarily perfused through the pulmonary capillaries in the healthy pigs, as expected, but that bronchial perfusion increased in the injured animals. This highly speculative finding will need to be addressed further in future studies. The net uptake rate and distribution volume of [^{68}Ga]Ga-DOTA-Siglec-9 was lower in the lungs of the ARDS animals as compared to the healthy ones. However, the respective values of K_i normalized for the total tissue perfusion (K_i/F) as determined from [^{15}O]water PET resulted in the 4-fold enhancement in the ARDS lungs. Moreover, the retention of [^{68}Ga]Ga-DOTA-Siglec-9 in the lung was also higher for the ARDS pigs.

The lung samples immunohistochemically stained with an anti-VAP-1 antibody (1B2) showed that the positive signal was located near to the endothelial cell surface in the ARDS animals, whereas in the healthy controls, VAP-1 was still stored within the endothelial cell granules, as it had been observed in other experiments of tissue inflammation [8]. Thus, the immunohistochemistry assay demonstrated minor expression of VAP-1 on the endothelial surface and the kinetic modeling of [^{68}Ga]Ga-DOTA-Siglec-9 distribution together with the normalization to the perfusion showed higher net influx rate in the injured lungs. Therefore, these results indicate the potential of [^{68}Ga]Ga-DOTA-Siglec-9 PET-CT for the detection of lung inflammation in ARDS. However, the physiological expression of VAP-1 in pig lungs resulted in a dominating uptake of [^{68}Ga]Ga-DOTA-Siglec-9 masking the modest VAP-1 binding related to the inflammation. Consequently,

accurate detection of pig lung inflammation with [^{68}Ga]Ga-DOTA-Siglec-9 PET requires combination of kinetic modeling and tissue perfusion data at least in this animal model. If such a demanding protocol is also needed in patients, it might hamper the use of this promising method as routine clinical application for diagnosing pulmonary inflammation.

Conclusions

The kinetic modeling and normalization for the tissue perfusion measured by [^{15}O]water PET demonstrated 4-fold higher net uptake rate of [^{68}Ga]Ga-DOTA-Siglec-9 in the acute lung inflammation in pigs as compared to healthy controls. Without the kinetic modeling and normalization, [^{68}Ga]Ga-DOTA-Siglec-9 uptake was 2-fold higher in the lungs of healthy pigs. Thus, VAP-1 mediated detection of acute lung inflammation requires combination of [^{68}Ga]Ga-DOTA-Siglec-9 PET-CT, [^{15}O]water PET, and kinetic modeling.

Acknowledgements

Marie Ahlman, Annie Bjurebäck, Monica Hall, Mimmi Lidholm, Lars Lindsjö, Anders Nordgren, and Agneta Roneus are greatly appreciated for the technical assistance in performing the scans and handling animals. Sari Mäki is thanked for her help in immunohistochemistry assays and Anne Sovikoski-Georgieva is thanked for secretarial help. This research was financially supported by the Swedish Heart and Lung foundation and by the Swedish Research Council (K2015-99X-22731-01-4) as well as Academy of Finland. JR receives support from Beca Cotutela Doctoral CONICYT.

Address correspondence to: Dr. Irina Velikyan, PET-Center, Center for Medical Imaging, Uppsala University Hospital, SE-751 85 Uppsala, Sweden. Tel: +46 (0)70 4834137; Fax: +46 (0)18 6110619; E-mail: irina.velikyan@bms.uu.se

References

[1] Matthay MA and Zemans RL. The acute respiratory distress syndrome: pathogenesis and treatment. Annu Rev Pathol 2011; 6: 147-163.

[2] Ware LB. Pathophysiology of acute lung injury and the acute respiratory distress syndrome. Semin Respir Crit Care Med 2006; 27: 337-349.

[3] Rhodes CG and Hughes JM. Pulmonary studies using positron emission tomography. Eur Respir J 1995; 8: 1001-1017.

[4] de Prost N, Tucci MR and Melo MF. Assessment of lung inflammation with 18F-FDG PET during acute lung injury. AJR Am J Roentgenol 2010; 195: 292-300.

[5] Costa EL, Musch G, Winkler T, Schroeder T, Harris RS, Jones HA, Venegas JG and Vidal Melo MF. Mild endotoxemia during mechanical ventilation produces spatially heterogeneous pulmonary neutrophilic inflammation in sheep. Anesthesiology 2010; 112: 658-669.

[6] Roivainen A, Jalkanen S and Nanni C. Gallium-labelled peptides for imaging of inflammation. Eur J Nucl Med Mol Imaging 2012; 39 Suppl 1: S68-77.

[7] Autio A, Jalkanen S and Roivainen A. Nuclear imaging of inflammation: Homing-associated molecules as targets. EJNMMI Res 2013; 3: 1-7.

[8] Lankinen P, Makinen TJ, Poyhonen TA, Virsu P, Salomaki S, Hakanen AJ, Jalkanen S, Aro HT and Roivainen A. 68Ga-DOTAVAP-P1 PET imaging capable of demonstrating the phase of inflammation in healing bones and the progress of infection in osteomyelitic bones. Eur J Nucl Med Mol Imaging 2008; 35: 352-364.

[9] Autio A, Henttinen T, Sipila HJ, Jalkanen S and Roivainen A. Mini-PEG spacering of VAP-1-targeting 68Ga-DOTAVAP-P1 peptide improves PET imaging of inflammation. EJNMMI Res 2011; 1: 10.

[10] Autio A, Ujula T, Luoto P, Salomaki S, Jalkanen S and Roivainen A. PET imaging of inflammation and adenocarcinoma xenografts using vascular adhesion protein 1 targeting peptide 68Ga-DOTAVAP-P1: comparison with 18F-FDG. Eur J Nucl Med Mol Imaging 2010; 37: 1918-1925.

[11] Ujula T, Salomaki S, Virsu P, Lankinen P, Makinen TJ, Autio A, Yegutkin GG, Knuuti J, Jalkanen S and Roivainen A. Synthesis, Ga-68 labeling and preliminary evaluation of DOTA peptide binding vascular adhesion protein-1: a potential PET imaging agent for diagnosing osteomyelitis. Nucl Med Biol 2009; 36: 631-641.

[12] Autio A, Vainio PJ, Suilamo S, Mali A, Vainio J, Saanijoki T, Noponen T, Ahtinen H, Luoto P, Teras M, Jalkanen S and Roivainen A. Preclinical evaluation of a radioiodinated fully human antibody for in vivo imaging of vascular adhesion protein-1-positive vasculature in inflammation. J Nucl Med 2013; 54: 1315-1319.

[13] Aalto K, Autio A, Kiss EA, Elima K, Nymalm Y, Veres TZ, Marttila-Ichihara F, Elovaara H, Saanijoki T, Crocker PR, Maksimow M, Bligt E, Salminen TA, Salmi M, Roivainen A and Jalkanen S. Siglec-9 is a novel leukocyte ligand for vascular adhesion protein-1 and can be used in PET imaging of inflammation and cancer. Blood 2011; 118: 3725-3733.

[14] Ahtinen H, Kulkova J, Lindholm L, Eerola E, Hakanen AJ, Moritz N, Soderstrom M, Saanijoki T, Jalkanen S, Roivainen A and Aro HT. (68) Ga-DOTA-Siglec-9 PET/CT imaging of peri-implant tissue responses and staphylococcal infections. EJNMMI Res 2014; 4: 45.

[15] Virtanen H, Autio A, Siitonen R, Liljenback H, Saanijoki T, Lankinen P, Makila J, Kakela M, Teuho J, Savisto N, Jaakkola K, Jalkanen S and Roivainen A. (68)Ga-DOTA-Siglec-9 - a new imaging tool to detect synovitis. Arthritis Res Ther 2015; 17: 308.

[16] Borges JB, Costa EL, Suarez-Sipmann F, Widstrom C, Larsson A, Amato M and Hedenstierna G. Early inflammation mainly affects normally and poorly aerated lung in experimental ventilator-induced lung injury*. Crit Care Med 2014; 42: e279-287.

[17] Velikyan I. Synthesis, Characterization and Application of ^{68}Ga-Labelled Macromolecules Doctorate thesis 2005; http://urn.kb.se/resolve?urn=urn:nbn:se:uu:diva-5876.

[18] Velikyan I, Beyer GJ and Langstrom B. Microwave-supported preparation of ^{68}Ga-bioconjugates with high specific radioactivity. Bioconjug Chem 2004; 15: 554-560.

[19] Suarez-Sipmann F, Santos A, Peces-Barba G, Bohm SH, Gracia JL, Calderon P and Tusman G. Pulmonary artery pulsatility is the main cause of cardiogenic oscillations. J Clin Monit Comput 2013; 27: 47-53.

[20] Borges JB, Costa EL, Bergquist M, Lucchetta L, Widstrom C, Maripuu E, Suarez-Sipmann F, Larsson A, Amato MB and Hedenstierna G. Lung inflammation persists after 27 hours of protective acute respiratory distress syndrome network strategy and is concentrated in the nondependent lung. Crit Care Med 2015; 43: e123-132.

[21] Watson CC. New, faster, image-based scatter correction for 3D PET. IEEE Trans Nucl Sci 2000; 47: 1587-1594.

[22] Jaakkola K, Nikula T, Holopainen R, Vahasilta T, Matikainen MT, Laukkanen ML, Huupponen R, Halkola L, Nieminen L, Hiltunen J, Parviainen S, Clark MR, Knuuti J, Savunen T, Kaapa P, Voipio-Pulkki LM and Jalkanen S. In vivo detection of vascular adhesion protein-1 in experimental inflammation. Am J Pathol 2000; 157: 463-471.

[23] de Winter JCF. Using the Student's t-test with extremely small sample sizes. Practical Assessment, Research & Evaluation 2013; 18.

[24] Bellani G, Messa C, Guerra L, Spagnolli E, Foti G, Patroniti N, Fumagalli R, Musch G, Fazio F and Pesenti A. Lungs of patients with acute respiratory distress syndrome show diffuse inflammation in normally aerated regions: a [18F]-fluoro-2-deoxy-D-glucose PET/CT study. Crit Care Med 2009; 37: 2216-2222.

[25] Musch G, Bellani G, Vidal Melo MF, Harris RS, Winkler T, Schroeder T and Venegas JG. Relation between shunt, aeration, and perfusion in experimental acute lung injury. Am J Respir Crit Care Med 2008; 177: 292-300.

[26] Wellman TJ, Winkler T, Costa EL, Musch G, Harris RS, Zheng H, Venegas JG and Vidal Melo MF. Effect of local tidal lung strain on inflammation in normal and lipopolysaccharide-exposed sheep*. Crit Care Med 2014; 42: e491-500.

[27] Salmi M, Kalimo K and Jalkanen S. Induction and function of vascular adhesion protein-1 at sites of inflammation. J Exp Med 1993; 178: 2255-2260.

[28] Singh B, Tschernig T, van Griensven M, Fieguth A and Pabst R. Expression of vascular adhesion protein-1 in normal and inflamed mice lungs and normal human lungs. Virchows Arch 2003; 442: 491-495.

[29] Tohka S, Laukkanen M, Jalkanen S and Salmi M. Vascular adhesion protein 1 (VAP-1) functions as a molecular brake during granulocyte rolling and mediates recruitment in vivo. FASEB J 2001; 15: 373-382.

[30] Vainio PJ, Kortekangas-Savolainen O, Mikkola JH, Jaakkola K, Kalimo K, Jalkanen S and Veromaa T. Safety of blocking vascular adhesion protein-1 in patients with contact dermatitis. Basic Clin Pharmacol Toxicol 2005; 96: 429-435.

[31] Fan E, Villar J and Slutsky AS. Novel approaches to minimize ventilator-induced lung injury. BMC Med 2013; 11: 85.

[32] Murata M, Noda K, Fukuhara J, Kanda A, Kase S, Saito W, Ozawa Y, Mochizuki S, Kimura S, Mashima Y, Okada Y and Ishida S. Soluble vascular adhesion protein-1 accumulates in proliferative diabetic retinopathy. Invest Ophthalmol Vis Sci 2012; 53: 4055-4062.

[33] Ataseven A and Kesli R. Novel inflammatory markers in psoriasis vulgaris: vaspin, vascular adhesion protein-1 (vap-1), and ykl-40. G Ital Dermatol Venereol 2014; [Epub ahead of print].

[34] Aalto K, Maksimow M, Juonala M, Viikari J, Jula A, Kahonen M, Jalkanen S, Raitakari OT and Salmi M. Soluble vascular adhesion protein-1 correlates with cardiovascular risk factors and early atherosclerotic manifestations. Arterioscler Thromb Vasc Biol 2012; 32: 523-532.

[35] Bhattacharya J, Gropper MA and Shepard JM. Lung expansion and the perialveolar interstitial pressure gradient. J Appl Physiol (1985) 1989; 66: 2600-2605.